ACS APPLIED MATERIALS & INTERFACES

Research Article

www.acsami.org

Preparation and Characterization of Conductive and Transparent Ruthenium Dioxide Sol–Gel Films

John S. Allhusen and John C. Conboy*

Department of Chemistry, University of Utah , 315 South 1400 East, Salt Lake City, Utah 84112, United States

Supporting Information

ABSTRACT: RuO_2 conductive thin films were synthesized using the sol–gel method and deposited onto transparent insulating substrates. The optical transmission, film thickness, surface morphology and composition, resistivity, and spectroelectrochemical performance have been characterized. The optical transmission values of these films ranged from 70 to 89% in the visible region and from 56 to 88% in the infrared region. Resistivity values of the RuO_2 sol–gel films varied from 1.02×10^{-3} to 1.13 Ω cm and are highly dependent on the initial solution concentration of RuO_2 in the sol–gel. The RuO_2 sol–gel films were used as electrodes for the electrochemical oxidation and reduction of ferrocenemethanol. The electrochemical behavior of our novel RuO_2 sol–gel films was compared to that of a standard platinum disk electrode and showed no appreciable differences in the half-wave potential ($E_{1/2}$). The mechanical and chemical stability of the coatings was tested by physical abrasion and exposure to highly acidic, oxidizing Piranha solution. Repeated exposure to these extreme conditions did not result in any appreciable decline in electrochemical performance. Finally, the use of the novel RuO_2 sol–gel conductive and transparent films was demonstrated in a spectroelectrochemistry experiment in which the oxidation and reduction of ferrocenemethanol was monitored via UV–vis spectroscopy as the applied potential was cycled.

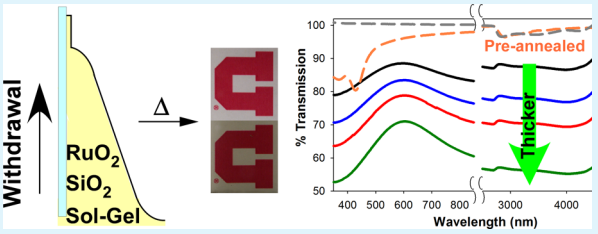

KEYWORDS: *sol–gel, ruthenium dioxide, thin film, electrochemistry, spectroelectrochemistry, X-ray photoelectron spectroscopy*

INTRODUCTION

Optically transparent conductive materials have played a critical role in the energy and electronic industries over the past decade. One of the most common and well characterized materials in these industries is indium tin oxide (ITO). ITO is a particularly valuable material for thin conductive films due to its high conductivity and transparency.[1−5] It is used in liquid crystal displays, photovoltaic cells, and a variety of other electronic devices. Although there are multiple applications for ITO, there are a number of drawbacks, such as the cost and inefficiency of the manufacturing process and the ease with which the film may be etched in oxidative environments.[1,2,5,6] Alternatives to ITO include carbon nanotubes, graphene films, metal meshes, and other metal oxide combinations.[1,6−13] Carbon nanotubes and graphene films have been successfully applied to flexible substrates, but they are also unstable in highly oxidizing environments as well as difficult to apply to a flat, insulating, glass substrate.[1,6] Ruthenium dioxide (RuO_2) is another appealing compound for creating optically transparent conductive materials because of its high electronic conductivity at room temperature and resistance to chemical oxidation.[14]

In 2009, Chervin et al. demonstrated the ability to deposit ruthenium dioxide (RuO_2) particles onto a flexible, insulating substrate of silica paper resulting in a crust of RuO_2 conductive particles on the surface of the substrate.[15,16] A subambient precursor solution of RuO_4 was allowed to thermally decompose to RuO_2 nanoparticles in solution at room temperature. These nanoparticles were then allowed to physisorb onto a substrate.[15,16] The resulting RuO_2 nanoskins exhibited conductivity values ranging from 14 to 830 mS cm^{-1}. The conductivity was also found to be dependent on the temperature at which the films were annealed.[16] This RuO_2 direct deposition method has also been employed by Long et al. to create conductive films on titanium foil and a variety of transparent substrates resulting in films with conductivities on the order of 1×10^3 S cm^{-1} and visible transmission values as high as 85%.[17,18] However, the method of depositing ruthenium dioxide onto insulating substrates developed by Chervin et al. results in a high level of film variability from deposition to deposition, and produces films with a wide range of measured sheet resistance values (1000 to 5000 Ω).[17] In addition, the deposited films lack mechanical strength and can easily be removed with gentle abrasion. Development of a method for creating conductive and transparent RuO_2 films in a convenient, low cost and highly reproducible manner with increased stability (chemical and mechanical) would be very beneficial.

Jeng et al. have described a more reproducible method to create conductive RuO_2 films, involving the incorporation of RuO_2 particles into a silica dioxide (SiO_2) sol–gel matrix.[19] The resistivity of the coatings reported by Jeng et al. varies from ~1×10^{-1} to 1×10^{-3} Ω cm with optical transmission values

Received: August 9, 2013
Accepted: October 22, 2013
Published: November 12, 2013

reported from 55 to 90%.[19] An increase in the ratio of Ru/Si in the sol–gel was accompanied by a decrease in resistivity and transmission. The sol–gel procedure for creating RuO_2 films is easily customizable, allowing for control of the transparency and conductivity of the deposited film.[20] In addition, there are many different SiO_2 precursor compounds to choose from when attempting to synthesize sol–gel materials.[21] If high optical quality sol–gel films are desired, a previous study published by Yang et al. reported that the use of a methyl alkoxide precursor and silica tetrachloride ($SiCl_4$) as a catalyst resulted in films with low optical loss (<0.2 dB/cm) and highly homogeneous films compared to sol–gels catalyzed with HCl, which was used by Jeng et al.[22,23]

The work described in this article utilizes a method of producing optically transparent conductive RuO_2 films on glass substrates using the methyl alkoxide precursor methyltriethoxysilane (MTES) and $SiCl_4$ as a catalyst to create a sol–gel material with high conductance and excellent optical properties. The films were deposited through a dip-coating procedure, which also has the ability to coat substrates with curved surfaces. The resulting films were characterized using a variety of surface techniques to examine thickness, roughness, and surface composition. The optical properties were explored in both the infrared and visible regions. These novel films were then tested as electrodes for spectroelectrochemistry and their electrochemical performance was compared with a standard platinum disk electrode. Robustness of the sol–gel films was tested by exposing the electrodes to a highly oxidizing environment of 70% H_2SO_4–30% H_2O_2 v/v (Piranha) solution. The thorough characterization conducted in this study demonstrates that an optically transparent conductive material can be reliably and efficiently created using simple sol–gel dip-coating methods. The resulting films are extremely stable and resistant to oxidation and acidic conditions.

EXPERIMENTAL SECTION

Sol–Gel Preparation. Absolute ethanol (200 proof) was obtained from Decon Laboratories. Methyltriethoxysilane (MTES) and silicon tetrachloride ($SiCl_4$) were obtained from Sigma Aldrich. ***Caution!*** *MTES is a flammable liquid and should be kept away from ignition sources. $SiCl_4$ is extremely toxic when inhaled; handle this material under proper ventilation conditions.* Ruthenium trichloride x-hydrate ($RuCl_3 \cdot xH_2O$) was obtained from Alfa Aesar. ***Caution!*** *$RuCl_3 \cdot xH_2O$ causes severe skin burns and eye damage upon contact; proper protection should be used when handling this product.* All chemicals were used as received and without further purification. Premiere brand silica microscope slides were used as the substrate for deposition of the films. The slides were first cleaned with Alconox cleaning detergent, and then rinsed sequentially with 18 MΩ cm Nanopure water, isopropanol, ethanol, and Nanopure water. The substrates were then submerged in a solution of 70% H_2SO_4–30% H_2O_2 v/v (Piranha) for a minimum of eight hours. ***Caution!*** *Piranha is a highly reactive solution which will react violently with organic materials and metals; care should be taken when handling this material.* After treatment in Piranha, the slides were thoroughly rinsed with Nanopure water and submerged in a 100 mM HCl solution for a minimum of 3 h. Once removed, the slides were rinsed thoroughly with Nanopure water and then ozone cleaned (Jelight UVO Cleaner) for five minutes.

The RuO_2:SiO_2 sol–gels were synthesized from two precursor solutions. Initially MTES and $SiCl_4$ were added, in a 6:1 molar ratio to 10 mL of absolute ethanol. This solution was stirred constantly for 2 h. A separate precursor solution containing 0.5, 1, 2, or 4 mmol of $RuCl_3 \cdot xH_2O$ dissolved in 10 mL of absolute ethanol was stirred for one hour. The two precursor solutions were combined together and then stirred constantly for one hour. The final solutions contained a molar ratio of 24:6:1 $RuCl_3 \cdot xH_2O$:MTES:$SiCl_4$ (3.43:1 Ru:Si), 12:6:1 $RuCl_3 \cdot xH_2O$:MTES:$SiCl_4$ (1.71:1 Ru:Si), 6:6:1 $RuCl_3 \cdot xH_2O$:MTES:$SiCl_4$ (0.83:1 Ru:Si) or 3:6:1 $RuCl_3 \cdot xH_2O$:MTES:$SiCl_4$ (0.43:1 Ru:Si). The sol–gel was allowed to age for a minimum of 48 h in a sealed container prior to dip coating.

A KSV Minitrough substrate dipper was used for dip coating the silica slides with the sol–gel. The substrates were withdrawn at speeds of 8.5 and 4.2 cm/min. The coated substrates were allowed to dry under ambient conditions before the annealing process. Each sample was then annealed at a temperature of 450 °C for 15 min. The samples were then slowly cooled to room temperature in the furnace before use.

Characterization. *Thickness.* The thickness of the sol–gel films was determined using ellipsometry. For the ellipsometric measurements, sol–gel films were deposited on p-type silicon wafers (Silicon Quest International) and the thickness was determined using a J.A Woollam variable angle spectroscopic ellipsometer. The p-type silicon wafers used as a substrate were cleaned using the method described above for the glass slides.

Optical Transmission. A Perkin–Elmer Spectrum One FT–IR spectrometer and Lambda 25 UV–vis spectrophotometer were used to examine the transparency of the deposited coatings in the infrared and ultraviolet–visible regions respectively. The transmission in the infrared was recorded from 2000 to 4000 cm^{-1} and transmission in the visible was recorded from 350 to 850 nm. For each spectrum collected, a clean silica slide served as the background.

IR spectra were recorded for bulk sol–gel materials. The precursor solutions were gently heated to ∼120 °C until all of the solvent was removed. A small amount (0.020 g) of the resulting solid was combined with 1.98 g KBr using a mortar and pestle. The amount of powder used to make a pellet was 0.100 g, yielding a pellet with a thickness <1 mm. A small amount of the 3.43:1 Ru:Si solid powder was annealed at 450 °C for 15 min. A blank spectrum was recorded using KBr without any sol–gel material. Spectra were baseline corrected and fit using Grams AI software.

Surface Characterization. A Bruker Dimension Icon atomic force microscope (AFM) was used to characterize the surface roughness of the as-prepared sol–gel film. Images were collected using PeakForce Quantitative Nanomechanical Property Mapping mode (PeakForce QNM). A silicon tip on a nitride cantilever with a force constant of k = 0.4 N/m was used for imaging. Images were collected for each sample as well as an uncoated clean silica slide and the root-mean-square (RMS) roughness was determined. Several topographical images were collected at various positions on the sample in order to obtain a statistical average of the RMS roughness.

X-ray photoelectron spectroscopy (XPS) was used to determine the surface composition of the sol–gel films. Sol–gel films were prepared on p-type silicon wafers for analysis. A Kratos AXIS Ultra DLD X-ray photoelectron spectrometer was used to collect the XPS data. A monochromatic aluminum kα source at 1486.6 eV was used to excite electrons within the sample. Initial survey scans were collected at a pass energy of 160 eV and high resolution scans were collected at 40 eV. The measured peak resolution for this instrument is 0.7 eV for a smooth, conductive silver surface. XPS data were collected for as-prepared sol–gel films before and after sputtering with an argon source for 30 s. The sample area examined was 700 × 300 μm. Several spectra were taken at various positions in the sample in order to obtain a statistical average of the surface composition of the sample.

Conductivity. The resistivity of the sol–gel films was measured using a four-wire resistance measurement (Keithley 2000 multimeter). Copper wire leads were attached to the surface of the sol–gel films with silver epoxy (Alfa Aesar). A line of silver epoxy was applied at each end of the coating spanning the width of the coating allowing for the resistance to be measured across the entirety of the coated film. The four-wire configuration forces a test current through the sample and measures the resistance with a set of test leads, whereas the voltage across the sample is measured through a second set of leads (sense leads). This setup allows for a more accurate determination of resistance by excluding the voltage drop that may be present in the test leads.

Table 1. Thickness, RMS Surface Roughness, Resistivity, Optical Transmission, and Surface Composition of the Annealed RuO_2 Sol−Gel Films

withdrawal speed (cm/min)	Ru:Si (solution)	thickness (nm)	RMS surface roughness (nm)	resistivity (Ω cm)	% T at 600 nm	Ru:Si (surface)
8.5	0.43:1				97.4	
8.5	0.86:1	(9.63)		1.134	93.4	0.1 ± 0.1:1
8.5	1.71:1	9.6 ± 0.2	0.7	1.02×10^{-3}	83.5	0.4 ± 0.1:1
8.5	3.43:1	16.0 ± 0.8	0.7	1.03×10^{-3}	71.0	1.0 ± 0.2:1
4.2	1.71:1	7.5 ± 0.7	0.7	1.72×10^{-3}	88.5	
4.2	3.43:1	11.4 ± 0.1	1.2	1.24×10^{-3}	78.9	

Electrochemistry. A Princeton Applied Research (PAR) 273 potentiostat was used for all electrochemical experiments. A standard solution of 0.9 mM ferrocenemethanol (FcMeOH, Sigma Aldrich) in 100 mM NaCl was prepared and degassed for 30 min with argon before electrochemical measurements were taken. Cyclic voltamograms (CVs) were collected from −200 to +650 mV, using a AglAgCl reference electrode and a platinum wire counter electrode. A reference CV was collected using a platinum disk working electrode (area = 2.011 mm^2, BASi), platinum wire counter electrode, and a AglAgCl reference electrode (BASi). The stability of the sol−gel coatings was tested by exposing the previously described sol−gel coated working electrode to Piranha solution five consecutive times for a minimum of 8 h per exposure. Cyclic voltammograms were collected after each Piranha exposure until the current reached a stable value.

The electroactive area of the platinum electrode was determined using the current obtained from the reduction of ferrocenemethanol. The platinum electrode was mechanically polished (Buehler Master Polish 2) and then thoroughly rinsed with methanol and Nanopure water. The Pt working electrode was then sonicated in Nanopure water for five minutes before use. The electroactive area of the RuO_2 sol−gel electrode was calculated by comparing the ratio of the integrated FcMeOH reduction current to the integrated FcMeOH reduction current measured using a platinum electrode.

Spectroelectrochemistry. The spectroelectrochemistry of ferrocenemethanol oxidation and reduction was measured using the three electrode setup described above and a Perkin−Elmer Lambda 25 spectrophotometer. Absorbance spectra were recorded while the applied potential was cycled between −200 to +650 mV at a scan rate of 1 mV/s. The sol−gel films containing 1.71:1 Ru:Si withdrawn at a speed of 8.5 cm/min were used for all the spectroelectrochemical experiments. The wavelength region probed by the UV−vis spectrophotometer was 500 to 800 nm with a scan rate of 2880 nm/min, which corresponds to a spectrum collected every ∼25 mV. The instrument collected data in a double beam mode and the blank contained 100 mM NaCl and a 1.71:1 Ru:Si sol−gel coated silica slide.

RESULTS AND DISCUSSION

To fully characterize the performance of the novel RuO_2 sol−gel-derived material, several key physical properties were investigated; thickness, optical transmission, surface roughness, composition, and conductivity. The thickness of dip-coated sol−gel films is governed by the following equation for the dip coating processes:[20]

$$h = C\sqrt{\frac{\eta U_o}{\rho g}} \quad (1)$$

where h is the film thickness, C is a constant, η is the viscosity of the solution, U_o is the withdrawal rate, ρ is the density of the solution and g is the gravitational force constant.[20] The thickness of the films is most easily adjusted by varying the withdrawal rate used for film deposition. Film thickness was determined by ellipsometry for the sol−gel films deposited on p-type silicon. Thickness values varied with solution composition and withdrawal speed and are reported in Table 1. The thickness values we measured range from 7.5 to 11.4 nm. These values are more than an order of magnitude lower than the values reported for sol−gel coatings prepared by Jeng et al. (∼140 nm).[19] However, these values are only two to three times higher than values obtained by Chervin et al. for direct deposition of RuO_2 nanoparticles (∼3 nm).[15]

Optical transmission characteristics of the sol−gel films are also highly dependent upon the withdrawal rate and fraction of ruthenium in the sol−gel. Figure 1A demonstrates that our technique results in a highly transparent coating applied to a glass substrate. The UV−vis and IR transmission spectra in Figure 1B were used to quantify the impact of ruthenium concentration and withdrawal rate on the optical transmission of the films. UV−vis spectra were recorded for both preannealed and annealed sol−gel films. A small peak is observed in the UV−vis spectra at ∼430 nm for the unannealed films and is likely due to the O → Ru charge transfer of the highly oxidized RuO_4 species formed in solution.[24] When the films are annealed, this absorbance decreases as RuO_4 is converted to RuO_2. A noticeable increase in absorption around 350 nm is observed with increasing film thickness. This increase stems from the increase in the RuOH content within the film,[25] which was verified by collecting a UV−vis spectrum for a sol−gel film prepared without any ruthenium. The appearance of the peak around 350 nm is not due to thin-film interference, which was verified by collecting a spectrum from 200 to 4800

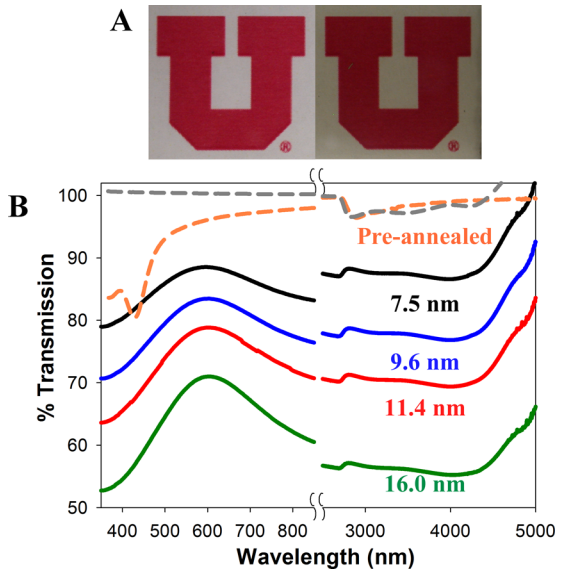

Figure 1. (A) Photograph of a silica slide coated with 1.71:1 Ru:Si sol−gel film withdrawn at 8.5 cm/min with a thickness of 9.6 nm. (B) Transmission spectra for preannealed and annealed RuO_2 sol−gel films of four different thicknesses. The spectrum for an annealed sol−gel without ruthenium is shown in gray for comparison.

nm on a fused silica substrate for a 3.43:1 Ru:Si film (see the Supporting Information). The IR spectra of the unannealed sol–gel films displays a broad absorbance at 2870 nm (3484 cm^{-1}) which is associated with the water in the sample. This peak disappears upon annealing resulting in a flat featureless spectrum from 2500 nm (4000 cm^{-1}) to 5000 nm (2000 cm^{-1}).

FT–IR spectra of bulk sol–gels were used to characterize the composition of the materials before and after annealing (Figure 2). The spectra have been normalized to the peak at 1100 cm^{-1}.

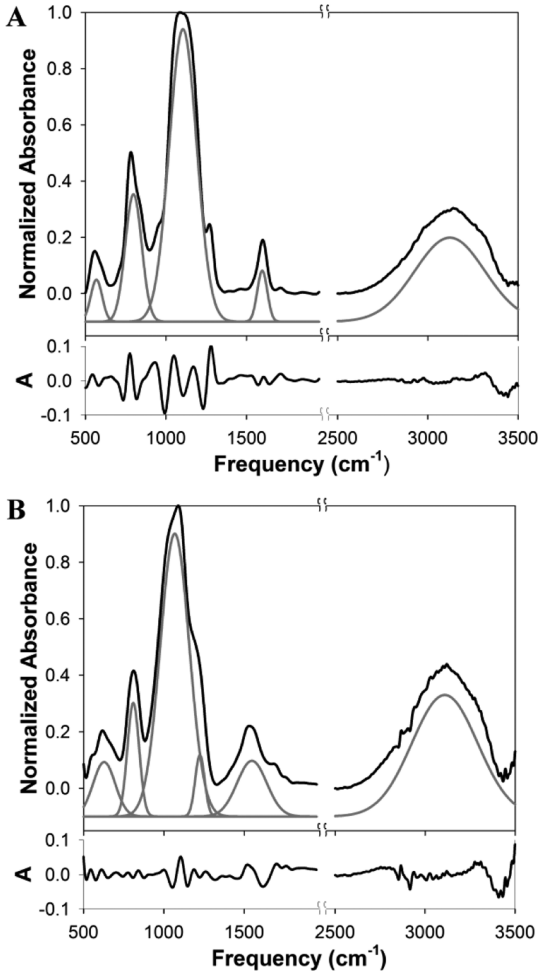

Figure 2. FTIR spectra of bulk (A) unannealed and (B) sol–gel material annealed at 450 °C for 15 min. The peak fits are offset by 0.1 absorbance units for clarity. The residuals for the peak fits are shown below each spectrum.

The annealed and unannealed materials show the same vibrational resonances. Vibrational modes were observed at 600, 800, 1100, 1600, and 3100 cm^{-1} for each sol–gel composition. The vibrational mode at 600 cm^{-1} is attributed to that of rutile RuO_2.[26,27] The peak around 800 cm^{-1} can be assigned to the Ru–O–Ru asymmetric stretch[26] or the Ru═O vibrational mode.[26,28] The broad peak at 1100 cm^{-1} is a combination of both Si–O–Si bonds[23,28] and RuOH vibrational stretches.[26] The vibrational band at 1600 cm^{-1} is a result of H–O–H stretching from water.[26,27] The peak at ∼3100 cm^{-1} is attributed to hydroxide species, either Si–OH or Ru–OH.[27,29] Upon annealing at 450 °C a peak begins to emerge around 1200 cm^{-1} that can be attributed to a secondary phase of silica as the films becomes denser.[23,28,30] The intensity or positions of the other vibrational modes do not change upon annealing.

We have compared the optical properties of the RuO_2 sol–gel films prepared here with other conductive and transparent materials. Hu et al. has reported the optical transmission characteristics for a variety of optically transparent conductive materials as a function of thickness.[31] The values presented by Hu et al. were used to calculate the transmission for films with thicknesses of 10 nm as a comparison to the RuO_2 sol–gel films in this study. For a carbon nanotube film with a thickness of 10 nm the transmission at 550 nm was 92%, whereas a graphene film had a transmission of 70% at the same wavelength and ITO films had a transmission of 99% at 550 nm.[31] The films reported in this study have transmissions of 71, 79, 84, and 89% at 600 nm depending on the Ru content and thickness. Similar RuO_2 sol–gel films created by Jeng et al. have calculated transmission values for 10 nm thick films ranging from 96 to 99% at 600 nm.[19]

The transmission characteristics in the infrared are of particular interest because highly conductive ITO films begin to absorb around 1000 nm.[9,31] The infrared transmission values described by Hu et al. at 3 μm calculated for a 10 nm thick film of carbon nanotubes, graphene or ITO were 96, 75, and 73%, respectively.[31] The RuO_2 sol–gel films described here maintain an average percent transmission from 56 to 88% at 3 μm and the transmission spectrum in the IR is nearly flat and featureless as seen in Figure 1. Infrared transmission values of the RuO_2 sol–gel films synthesized by Jeng et al. were not reported; however, they did report the decrease in OH stretching modes in annealed films as compared to preannealed films, as we have observed here.[19]

The surface morphology of the sol–gel samples was investigated to characterize the uniformity of the as-prepared sol–gel films. Surface morphology can significantly impact the optical and electrochemical behavior of the deposited film. For example, surface defects would create a discontinuity in the coating thereby increasing the resistance of the deposited films. AFM images are shown for a bare glass slide and a sol–gel film with the composition of 1.71:1 Ru:Si, Figure 3. The bare glass slide used as the substrate for the RuO_2 sol–gel films had an RMS surface roughness of 1.0 nm, whereas the deposited and annealed RuO_2 sol–gel film had a measured RMS surface roughness of 0.7 nm. Height histograms are shown for the entire surface area of both samples. The bare glass slide had a broader topographical distribution compared to the sol–gel-coated sample, which results in a larger RMS surface roughness value. The fact that these films are uniform and smooth across the measured area makes this material a promising transparent conductive film. Mapping the morphology of the films allows for the visualization of any defects present within the film, but does not provide any information on the composition at the surface of the film; for this, we turned to XPS analysis.

The surface composition of the RuO_2 sol–gel films was quantified using XPS. XPS spectra (Figure 4) are presented for films created with sol–gel solutions containing 0.83:1 Ru:Si, 1.71:1 Ru:Si and 3.43:1 Ru:Si withdrawn at rates of 8.5 cm/min and 4.2 cm/min. Initial survey scans were measured from 1200 to 0 eV at a pass energy of 160 eV to provide a broad compositional overview of the surface. In these survey scans, chlorine (B.E. ∼200 eV) is not detected (see the Supporting Information). The Ru 3d doublet is depicted in Figure 4 for the 3.43:1 Ru:Si, 1.71:1 Ru:Si, and 0.83:1 Ru:Si sol–gel films. The

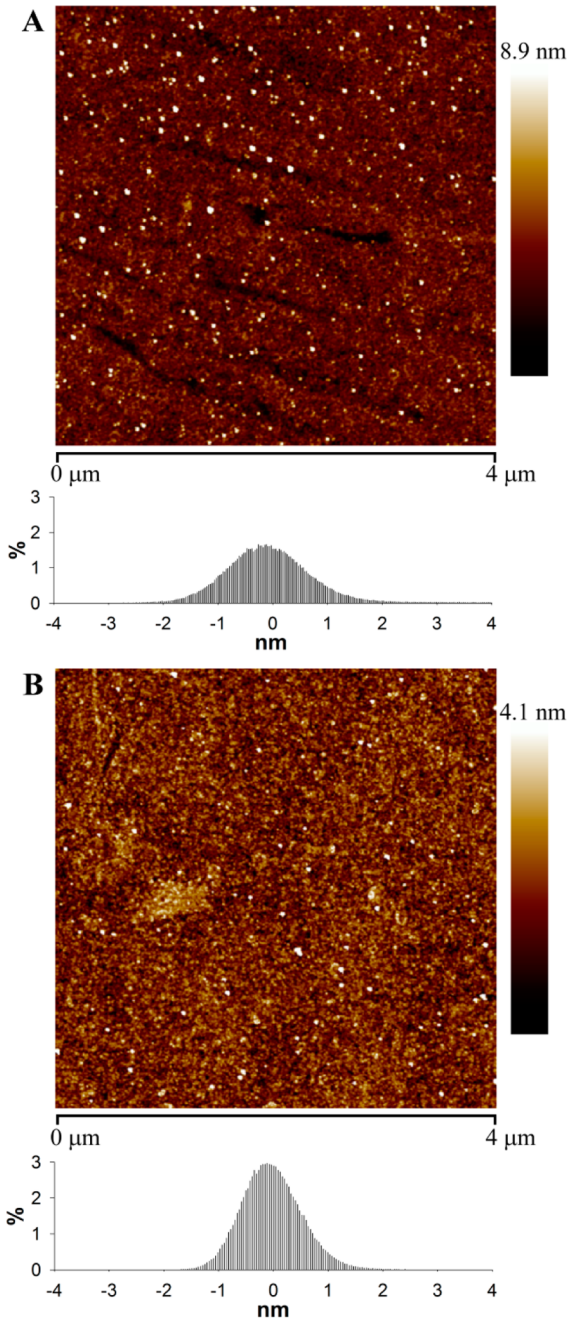

Figure 3. AFM images of (A) a bare glass slide and (B) a 1.71:1 Ru:Si sol–gel-coated glass slide. Height histograms are shown for each of the collected images.

Ru $3d_{5/2}$ peak at 280.5 eV has been previously assigned to RuO_2 and is the main ruthenium component within the synthesized films.[16,32−34] The shoulder at 282 eV is attributed to RuOH as previously reported by Chervin et al. for ruthenium nanoskins.[16] The peak at 285 eV is a composite of both Ru $3d_{3/2}$ and adventitious carbon on the surface.[16] The two peaks present within the Si 2p region are indicative of SiO_2 and Si metal located at 103 and 99 eV, respectively.[35,36] The Si metal peak is most likely due to exposure of the silicon wafer substrate after sputtering. The noticeable difference for the 3.43:1 Ru:Si sol–gel film withdrawn at 8.5 cm/min could be a result of measuring the bare substrate as this film had noticeable pore formations as imaged by AFM (data not shown). The O 1s binding energy at 532 eV is largely indicative of SiO_2 within the film with possible contributions from Si–OH.[16,35,37] The shoulder located at ~531 eV[16,26,34] is attributed to Ru–OH and RuO_2, which is consistent with the FTIR spectra discussed previously. As the ruthenium concentration increases within the film, the intensity of the shoulder at ~530 eV increases suggesting an increase in Ru–OH and RuO_2 species in the film. To determine the ratio of ruthenium and silica present at the surface, the excitation regions of the Ru 3d and Si 2p orbitals were measured. The Ru $3d_{5/2}$ and Si 2p peaks were fit with a Gaussian/Lorentzian function after the spectra were baseline corrected using Grams AI software.[38] Relative sensitivity factor (RSF) values were obtained from Briggs and Seah for Ru $3d_{5/2}$ and Si 2p.[38] The samples were cleaned by argon sputtering for 30 s to remove any adventitious carbon adsorption. After removal of any surface contaminants, the relative surface densities of Ru and Si were determined to be 0.4 ± 0.1:1 Ru:Si for films cast from the 1.71:1 Ru:Si solution and 1.0 ± 0.2:1 Ru:Si for films created from the 3.43:1 Ru:Si sol–gel solutions, respectively. These surface concentrations indicate that the surface is Si-rich with the possibility of the majority of ruthenium being located below the analyzed depth.

In addition to the surface properties, the resistivity of the Ru sol–gel films was calculated from the resistance measured using a four wire technique at a temperature of 25 °C, with the calculated values listed in Table 1. The films withdrawn at 8.5 cm/min with molar solution ratios of 3.43:1 Ru:Si, 1.71:1 Ru:Si, 0.83:1 Ru:Si, 0.43:1 Ru:Si had resistivity values of 1.03×10^{-3}, 1.02×10^{-3}, and 1.13 Ω cm and >1 GΩ, respectively. These values indicate that the resistivity of the sol–gel films is relatively constant for films deposited from solutions with a composition ≥1.71:1 Ru:Si. The reported resistivity values are within the range reported by Jeng et al. for their 30:1 Ru:Si sol–gel films.[19] Jeng et al. annealed their films in a nitrogen atmosphere,[19] which is known to inhibit the growth of RuO_2 particles as confirmed by Shimamura et al.[39] The sol–gel films prepared here were annealed under ambient atmospheric conditions allowing the RuO_2 particles to expand in size and become fully oxidized. This increase in particle size creates more contacts throughout the films causing the resistivity to decrease. It is important to note that the film with the lowest resistivity has a transmission value of ~84% at 600 nm, whereas the transmission achieved be Jeng et al.'s film of lowest resistivity of $\sim 9 \times 10^{-4}$ Ω cm was ~55% at 600 nm.[19] The RuO_2 sol–gel film with a solution composition of 1.71:1 Ru:Si, which was withdrawn at a rate of 8.5 cm/min is a prime candidate for spectroelectrochemical experiments due to the high optical transmission (>70%) throughout the visible region, and a modest resistivity of 1.02×10^{-3} Ω cm. In addition, sol–gel films prepared with this composition and withdrawal speed also possess the greatest surface uniformity as confirmed by AFM measurements.

The electrochemical performance of the sol–gel films was tested by measuring the reversible electrochemistry of a solution containing 0.9 mM ferrocenemethanol in 100 mM NaCl supporting electrolyte by cyclic voltammetry. The results were compared against cyclic voltammograms of ferrocenemethanol recorded with a platinum electrode (area = 2.011 mm^2) and have been normalized to the electroactive area of either the Pt WE or the RuO_2 sol–gel electrodes (area = 4.8 cm^2) depending on which electrode was the active working electrode. The recorded CVs (Figure 5) measured with the RuO_2 working electrodes were mathematically corrected to compensate for

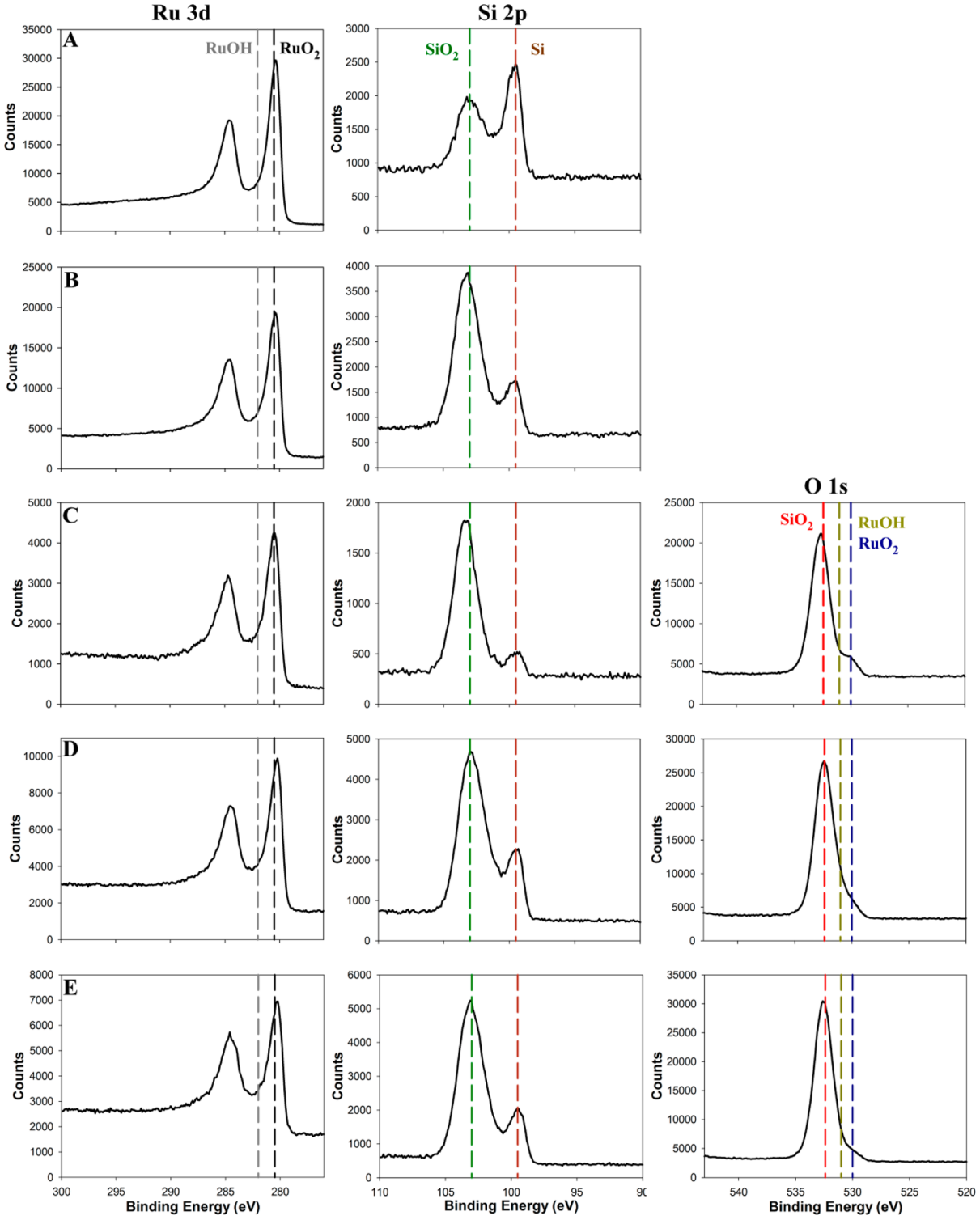

Figure 4. XPS spectra are given for the Ru 3d orbital, the Si 2p orbital, and the O 1s orbital for samples (A) 3.43:1 Ru:Si withdrawn at 8.5 cm/min, (B) 1.71:1 Ru:Si withdrawn at 8.5 cm/min, (C) 3.43:1 Ru:Si withdrawn at 4.2 cm/min, (D) 1.71:1 Ru:Si withdrawn at 4.2 cm/min, and (E) 0.83:1 Ru:Si withdrawn at 8.5 cm/min.

the resistance of the electrode using the values reported previously. The measured half-wave potential ($E_{1/2}$) for ferrocenemethanol at a Pt electrode was $E_{1/2}$ = 211 ± 2 mV versus AglAgCl and the peak separation measured for the Pt electrode was ΔE = 69 ± 2 mV. This value is above the value of ΔE = 59 mV for a one electron process due to the inherent solution resistance and possible surface contaminants that remained after the reported cleaning processes. The RuO_2 sol–gel electrode was cleaned in Piranha solution to remove any surface contaminants and CVs were recorded after each cleaning until the measured current stabilized. The final CV is shown in Figure 5 after the fifth consecutive cleaning in Piranha solution where the measured half-wave potential was $E_{1/2}$ = 206 ± 1 mV with a peak separation of ΔE = 83 ± 1 mV.

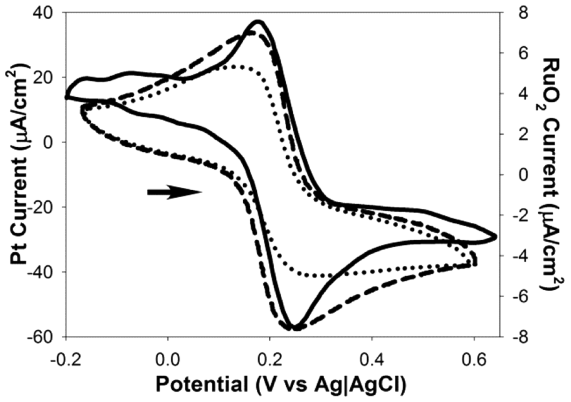

Figure 5. Solid line (——) is the CV collected with a Pt WE at a scan rate of 5 mV/s in 0.9 mM FcMeOH. The dotted line (●●●●●) is a CV collected using a RuO_2 sol–gel film as the WE. The dashed line (- - -) is a CV of the same RuO_2 sol–gel film after repeated cleanings in a Piranha solution. Scan direction is indicated by the arrow.

Similar electrochemical behavior for RuO_2 films has been demonstrated by Chervin et al. for RuO_2 particles deposited onto silica paper where they reported a peak separation of 76 mV for the reduction and oxidation peaks of ferricyanide.[15] The difference in the peak separation values between the Pt and RuO_2 sol–gel working electrodes can be attributed to the inherent capacitance of RuO_2.

The electroactive area for the clean RuO_2 sol–gel electrodes was calculated to be 32.0 ± 0.6%. This value was determined by integrating the normalized cathodic peak current for ferrocenemethanol recorded using the RuO_2 sol–gel electrode and then dividing this value by the integrated normalized cathodic current measured with a Pt working electrode. This value is consistent with the surface concentration of ruthenium determined by the previously described XPS measurements, which yielded a value for the surface concentration of ruthenium to be 30 ± 4%.

The mechanical and chemical stability of the synthesized RuO_2 sol–gel electrodes was tested by physical abrasion and multiple cleanings in highly oxidative Piranha solution, respectively. Physical abrasive tests included vigorously rubbing the substrate with a methanol soaked cloth and mechanical polishing using Buehler's Master Polish 2. The RuO_2 sol–gel films withstood rubbing with a methanol soaked cloth without any change in visible appearance or conductivity as measured by a 2-point probe. When mechanically polished by hand, the RuO_2 coatings required a period of time on the order of hours before complete removal of the sol–gel film from the substrate. The mechanical stability of the RuO_2 sol–gel films prepared here is similar to that observed for other thin conducting oxides such as ITO; however, the RuO_2 sol–gel films exhibit superior mechanical stability compared to carbon nanotubes[40] or graphene[41] films, which can peel away from the substrate under fluid flow. Exposing the RuO_2 sol–gel films to highly acidic Piranha solution did not damage the integrity of the films, but instead increased the electrochemical efficiency of the sol–gel films, as noted in the electrochemical experiments discussed above. The chemical stability of the synthesized RuO_2 films is exceptional compared to ITO which is known to easily etch in 0.2 M HCl.[42] When exposed to highly oxidizing Piranha solution, it was found that multiwalled carbon nanotubes become more oxidized and fragmented.[43] The oxidation of graphene films is known to proceed rapidly for single layer films when exposed to O_2 at temperatures <300 °C.[44] This oxidation causes holes in the film and can lead to irreversible damage.[44] The RuO_2 sol–gel films presented in this study exhibit outstanding mechanical and chemical stability, making them an appealing alternative to current thin film transparent conductive electrodes when a high level of robustness is required.

The ability of these electrodes to be used as substrates for spectroelectrochemistry experiments was also demonstrated. The RuO_2 sol–gel electrode was positioned at normal incidence to the light source in the UV–vis spectrometer. The spectrophotometer was configured in a double beam arrangement with an identical RuO_2 sol–gel electrode in 100 mM NaCl supporting electrolyte solution placed in the reference path to ensure that the measured response was due to redox changes to ferrocenemethanol and not the electrode itself. By monitoring the absorbance from 500 to 800 nm it was possible to observe the absorbance of the oxidized ferrocenemethanol species (FcMeOH+) at around ~625 nm.[45] The reduced form of ferrocenemethanol (FcMeOH) does not absorb within this region. Prior to recording spectra, the potential was cycled three times to establish a chemical equilibrium between FcMeOH and FcMeOH+. Figure 6 depicts the results of the spectroelectrochemistry experiments. These data are plotted as a function of the change in absorbance (z-axis) versus wavelength (x-axis) as the applied potential is scanned (y-axis). At negative applied potential, there is depletion in concentration of FcMeOH+ relative to the equilibrium concentration resulting in a negative value for the change in absorbance. As the scanned applied potential approaches the oxidation potential of E_{ox} = 247 ± 7 mV, evolution of FcMeOH+ starts to occur. This evolution increases drastically past E_{ox} continuing to increase the concentration of FcMeOH+, yielding an increase in the measured change in absorbance. The absorbance continues to increase as the potential is reversed until the reduction potential E_{red} = 164 ± 6 mV is approached. At this point, FcMeOH+ will become depleted as FcMeOH predominates in solution. The evolution of FcMeOH causes a decrease of the change in absorbance at ~625 nm as FcMeOH+ is depleted from the

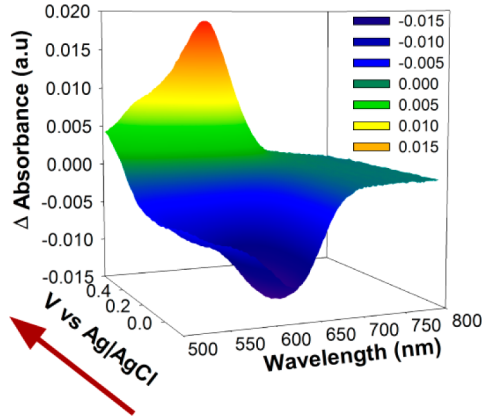

Figure 6. 3D spectra of absorbance versus wavelength and applied potential (ϕ) for a RuO_2 sol–gel electrode in 0.9 mM FcMeOH with 100 mM NaCl supporting electrolyte. The scan direction is indicated by the arrow. The evolution and depletion of oxidized FcMeOH+ is observable by the increase and decrease in absorbance as the applied potential is scanned.

system. The absorbance continues to decrease as the potential remains negative of E_{ox} because of the decrease in the concentration of FcMeOH. This spectroelectrochemical behavior continues as the potential is cycled. The application of the RuO_2 sol−gel films as electrodes in spectroelectrochemistry demonstrates the utility of these novel robust optically transparent conductive materials.

CONCLUSION

The RuO_2 sol−gel films synthesized in this report indicate promising potential for future implementation into a variety of optically transparent conductive devices. The optical transmission characteristics of these films are comparable to current alternative technologies and range from 70 to >90% in the visible region and from 50 to 90% in the infrared region. The infrared transmission profile is particularly impressive as no noticeable absorption occurs from 2000 to 4000 cm^{-1} making these films suitable for studying the effect of an applied potential on molecular chemistry in this region. The resistivity of these RuO_2 sol−gel films is easily tailored and is mostly dependent on the Ru precursor concentration and withdraw rate used for dip coating. The reported resistivity ranged from 1.134 to 1.02 × 10^{-3} Ω cm allowing for efficient use of these films as electrodes. The films are very robust and maintain their electrochemical integrity after multiple consecutive exposures to extreme acidic, oxidative environments. These films are completely viable alternatives for use in spectroelectrochemistry and optoelectronics because of their low-cost, long-term stability and high performance as transparent electrodes.

ASSOCIATED CONTENT

Supporting Information

UV−vis spectrum from 200 to 4800 nm for a 3.43:1 Ru:Si sol−gel film withdrawn at 8.5 cm/min deposited on quartz. XPS survey spectra for all samples listed. This material is available free of charge via the Internet at http://pubs.acs.org.

AUTHOR INFORMATION

Corresponding Author

*E-mail: conboy@chem.utah.edu.

Notes

The authors declare no competing financial interest.

ACKNOWLEDGMENTS

This work was funded by the National Science Foundation (NSF 1110351). J.S.A acknowledges Dr. Brian Van Devener for his assistance in the ellipsometry, AFM and XPS measurements. J.S.A. also acknowledges Dr. Jianing Sun and Andrea Donahue of J.A. Woollam Co. for their assistance in modeling the ellipsometry data to determine the thickness of the sol−gel films.

REFERENCES

(1) Granqvist, C. G. *Sol. Energy Mater. Sol. Cells* **2007**, *91*, 1529−1598.
(2) Fahland, M.; Karlsson, P.; Charton, C. *Thin Solid Films* **2001**, *392*, 334−337.
(3) Kim, H.; Gilmore, C. M.; Pique, A.; Horwitz, J. S.; Mattoussi, H.; Murata, H.; Kafafi, Z. H.; Chrisey, D. B. *J. Appl. Phys.* **1999**, *86*, 6451−6461.
(4) Kim, H.; Horwitz, J. S.; Kushto, G.; Pique, A.; Kafafi, Z. H.; Gilmore, C. M.; Chrisey, D. B. *J. Appl. Phys.* **2000**, *88*, 6021−6025.
(5) Tak, Y.-H.; Kim, K.-B.; Park, H.-G.; Lee, K.-H.; Lee, J.-R. *Thin Solid Films* **2002**, *411*, 12−16.
(6) Minami, T. *Thin Solid Films* **2008**, *516*, 5822−5828.
(7) de, H. W. A.; Bacsa, W. S.; Chatelain, A.; Gerfin, T.; Humphrey-Baker, R.; Forro, L.; Ugarte, D. *Science* **1995**, *268*, 845−7.
(8) Donner, S.; Li, H.-W.; Yeung, E. S.; Porter, M. D. *Anal. Chem.* **2006**, *78*, 2816−2822.
(9) Hecht, D. S.; Hu, L.-B.; Irvin, G. *Adv. Mater.* **2011**, *23*, 1482−1513.
(10) Mattevi, C.; Eda, G.; Agnoli, S.; Miller, S.; Mkhoyan, K. A.; Celik, O.; Mastrogiovanni, D.; Granozzi, G.; Garfunkel, E.; Chhowalla, M. *Adv. Funct. Mater.* **2009**, *19*, 2577−2583.
(11) Watcharotone, S.; Dikin, D. A.; Stankovich, S.; Piner, R.; Jung, I.; Dommett, G. H. B.; Evmenenko, G.; Wu, S.-E.; Chen, S.-F.; Liu, C.-P.; Nguyen, S. T.; Ruoff, R. S. *Nano Lett.* **2007**, *7*, 1888−1892.
(12) Wu, J.; Agrawal, M.; Becerril, H. A.; Bao, Z.; Liu, Z.; Chen, Y.; Peumans, P. *ACS Nano* **2010**, *4*, 43−48.
(13) Zheng, Q. B.; Gudarzi, M. M.; Wang, S. J.; Geng, Y.; Li, Z.; Kim, J.-K. *Carbon* **2011**, *49*, 2905−2916.
(14) Over, H. *Chem. Rev.* **2012**, *112*, 3356−3426.
(15) Chervin, C. N.; Lubers, A. M.; Pettigrew, K. A.; Long, J. W.; Westgate, M. A.; Fontanella, J. J.; Rolison, D. R. *Nano Lett.* **2009**, *9*, 2316−2321.
(16) Chervin, C. N.; Lubers, A. M.; Long, J. W.; Rolison, D. R. *J. Electroanal. Chem.* **2010**, *644*, 155−163.
(17) Long, J. W.; Owrutsky, J. C.; Chervin, C. N.; Rolison, D. R.; Melinger, J. S. *RuO_2 Coatings*. U.S. Patent 20 110 091 723, June 3, 2011.
(18) Rolison, D. R. U.S. Naval Research Laboratory, Washington, D.C., Personal Communication, 2011.
(19) Jeng, J.-S.; Lin, Y.-T.; Chen, J. S. *Thin Solid Films* **2010**, *518*, 5416−5420.
(20) Brinker, C. J.; Hurd, A. J.; Frye, G. C.; Shunk, P. R.; Ashley, C. S. *J. Ceram. Soc. Jpn.* **1991**, *99*, 862−77.
(21) Brinker, C. J., Scherer, G. W. *Sol−Gel Science*; Academic Press: San Diego, CA, 1990.
(22) Yang, L.; Saavedra, S. S. *Anal. Chem.* **1995**, *67*, 1307−14.
(23) Yang, L.; Saavedra, S. S.; Armstrong, N. R.; Hayes, J. *Anal. Chem.* **1994**, *66*, 1254−63.
(24) Neumann, R.; Khenkin, A. M. *Inorg. Chem.* **1995**, *34*, 5753−5760.
(25) Kitamura, R.; Pilon, L.; Jonasz, M. *Appl. Opt.* **2007**, *46*, 8118−8133.
(26) Ferrere, S.; A. Gregg, B. *J. Chem. Soc., Faraday Trans.* **1998**, *94*, 2827−2833.
(27) Patil, U. M.; Kulkarni, S. B.; Jamadade, V. S.; Lokhande, C. D. *J. Alloys Compd.* **2011**, *509*, 1677−1682.
(28) Park, S. K.; Kanjolia, R.; Anthis, J.; Odedra, R.; Boag, N.; Wielunski, L.; Chabal, Y. J. *Chem. Mater.* **2010**, *22*, 4867−4878.
(29) Zhu, H.; Ma, Y.; Fan, Y.; Shen, J. *Thin Solid Films* **2001**, *397*, 95−101.
(30) Tian, R.; Seitz, O.; Li, M.; Hu, W.; Chabal, Y. J.; Gao, J. *Langmuir* **2010**, *26*, 4563−4566.
(31) Hu, L.; Hecht, D. S.; Gruener, G. *Appl. Phys. Lett.* **2009**, *94*, 081103/1−081103/3.
(32) Chan, H. Y. H.; Takoudis, C. G.; Weaver, M. J. *J. Catal.* **1997**, *172*, 336−345.
(33) Iwasaki, Y.; Izumi, A.; Tsurumaki, H.; Namiki, A.; Oizumi, H.; Nishiyama, I. *Appl. Surf. Sci.* **2007**, *253*, 8699−8704.
(34) Kim, K. S.; Winograd, N. *J. Catal.* **1974**, *35*, 66−72.
(35) Miller, M. L.; Linton, R. W. *Anal. Chem.* **1985**, 2314−2319.
(36) Sirotti, F.; DeSantis, M.; Rossi, G. *Phys. Rev. B: Condens. Matter Mater. Phys.* **1993**, *48*, 8299−306.
(37) Barr, T. L. *J. Phys. Chem.* **1978**, *82*, 1801−10.
(38) *Practical Surface Analysis*; 2nd ed.; Briggs, D., Seah, M. P., Ed.; John Wiley and Sons: Chichester, England, 1996; Vol. *1*.
(39) Shimamura, A.; Huebert, T.; Thust, H. *Surf. Interface Anal.* **2004**, *36*, 1207−1209.

(40) Su, H.-C.; Chen, C.-H.; Chen, Y.-C.; Yao, D.-J.; Chen, H.; Chang, Y.-C.; Yew, T.-R. *Carbon* **2010**, *48*, 805−812.
(41) Soldano, C.; Mahmood, A.; Dujardin, E. *Carbon* **2010**, *48*, 2127−2150.
(42) Minami, T. *Semicond. Sci. Technol.* **2005**, *20*, S35−S44.
(43) Datsyuk, V.; Kalyva, M.; Papagelis, K.; Parthenios, J.; Tasis, D.; Siokou, A.; Kallitsis, I.; Galiotis, C. *Carbon* **2008**, *46*, 833−840.
(44) Liu, L.; Ryu, S.; Tomasik, M. R.; Stolyarova, E.; Jung, N.; Hybertsen, M. S.; Steigerwald, M. L.; Brus, L. E.; Flynn, G. W. *Nano Lett.* **2008**, *8*, 1965−1970.
(45) Zhu, Z.; Wang, M.; Gautam, A.; Nazor, J.; Morneu, C.; Prodanovic, R.; Schwaneberg, U. *Biotechnol. J.* **2007**, *2*, 241−248.